

## INVESTIGATING THE MECHANISM FOR THE FORMATION OF NITROUS OXIDE [N<sub>2</sub>O(*X*<sup>1</sup>Σ<sup>+</sup>)] IN EXTRATERRESTRIAL ICES

COREY S. JAMIESON,<sup>1</sup> CHRIS J. BENNETT,<sup>1</sup> ALEXANDER M. MEBEL,<sup>2</sup> AND RALF I. KAISER<sup>1,3,4</sup>

Received 2004 August 5; accepted 2004 December 19

### ABSTRACT

The formation of nitrous oxide, N<sub>2</sub>O(*X*<sup>1</sup>Σ<sup>+</sup>), in interstellar space and in ices on Pluto and Triton has been experimentally investigated. A molecular nitrogen (N<sub>2</sub>) and carbon dioxide (CO<sub>2</sub>) ice mixture was irradiated at 10 K with 5 keV electrons to simulate the electronic interaction effects of Galactic cosmic-ray bombardment of extraterrestrial ice samples over a time of 5 × 10<sup>6</sup> yr. By monitoring the experiment with a Fourier transform infrared spectrometer on line and in situ, the temporal evolution of the 2235 cm<sup>-1</sup> absorption band of nitrous oxide was found to follow pseudo-first-order kinetics. This indicates that the mechanism of formation is most likely a reaction between ground-state molecular nitrogen, N<sub>2</sub>(*X*<sup>1</sup>Σ<sub>g</sub><sup>+</sup>), and an oxygen atom, either in the ground state (<sup>3</sup>*P*) or in the first electronically excited state (<sup>1</sup>*D*), within the matrix cage through an addition of the oxygen atom to a non-bonding electron pair on the nitrogen molecule. The observation of nitrous oxide together with the kinetics and dynamics studies investigated in this paper underline the role of nonequilibrium processes in low-temperature ice matrices, aid in the understanding of chemical reaction pathways that exist in extraterrestrial ices, and assist a prospective identification of nitrous oxide on the surfaces of Pluto and Triton.

*Subject headings:* astrochemistry — infrared: ISM — infrared: solar system — ISM: abundances — ISM: molecules — molecular processes

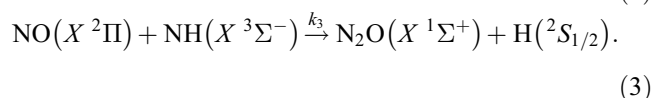
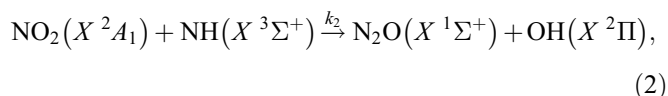
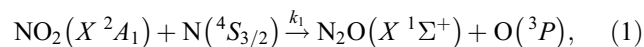
### 1. INTRODUCTION

In order to establish chemical reaction networks that simulate the chemical processing of extraterrestrial environments, it is necessary to understand the chemistry of nitrogen (Nejad et al. 1990; Sandford et al. 2001). The reactive diversity of this element ranges from the dark molecular clouds to protoplanetary disks of newly forming stars to the surfaces of bodies in the solar system (Pickles & Williams 1977; Charnley & Rodgers 2002). Of the 135 known molecules detected in the gas phase of the interstellar medium (ISM), almost 50 are nitrogen bearing.<sup>5</sup> This suggests that nitrogen has a rich chemistry that produces a variety of complex molecules. Even so, the great majority of interstellar nitrogen is likely to exist in the diatomic form (Womack et al. 1992; Snow 2004). However, molecular nitrogen, N<sub>2</sub>(*X*<sup>1</sup>Σ<sub>g</sub><sup>+</sup>), is a diatomic molecule with an inversion center, which means that the most abundant nitrogen-containing molecule is inactive in the microwave and infrared spectral regions. As these are our primary methods for remotely identifying rotations and vibrations in molecular species in the gas phase, our knowledge of the abundance of diatomic nitrogen in space is still limited. The recent gas-phase detection of molecular nitrogen in the far ultraviolet toward HD 124314, a moderately reddened star in the southern constellation of Centaurus, also underlines that the nitrogen chemistry in the interstellar medium is far from being understood (Knauth et al. 2004).

Cruikshank et al. (1993) and Owen et al. (1993) have observed the solid-state nitrogen molecule in the infrared using the first overtone of the ν<sub>1</sub> stretching mode centered at 4656 cm<sup>-1</sup> (Bernstein & Sandford 1999; Sandford et al. 2001). Both groups

were able to identify nitrogen ice as the primary surface component of Pluto and Triton (Neptune’s largest moon). Over 98% of the surface of these bodies is thought to be covered by nitrogen ice, leading to a chemistry dominated by the nitrogen molecule. While detecting solid nitrogen works for these surfaces, it would not suffice for the grains of the interstellar medium because of either a low abundance of nitrogen ice on grains, a low column density of grains along the line of sight, and/or insufficient enhancement of the absorption coefficient of the symmetry-forbidden ν<sub>1</sub> vibration of the nitrogen molecule.

A way to indirectly see the nitrogen molecule is to identify a nitrogen-containing species that could be used as a tracer for the nitrogen abundance in the ISM (Hudson & Moore 2002). One such molecule is N<sub>2</sub>O(*X*<sup>1</sup>Σ<sup>+</sup>), nitrous oxide, as suggested by Ehrenfreund et al. (1997). It has been observed in the gas phase of the Sgr B2 complex, regions N and M, which are dense, higher temperature regions within the Sagittarius cold molecular cloud (Halfen et al. 2001). Although efficient ion-molecule pathways that form nitrous oxide do not exist (Anicich & Huntress 1986; Le Teuff et al. 2000), the elevated temperatures present in the Sgr B2(N) core allow neutral-neutral reactions to proceed at a nonnegligible rate. According to Halfen et al. (2001), there exist three reactions that hold rate constants greater than 10<sup>-12</sup> cm<sup>3</sup> s<sup>-1</sup> for the production of nitrous oxide:



However, the first two reactions may not be important, since nitrogen dioxide has yet to be detected in the Sgr B2(N)

<sup>1</sup> Department of Chemistry, University of Hawaii at Manoa, Honolulu, HI 96822.

<sup>2</sup> Department of Chemistry and Biochemistry, Florida International University, Miami, FL 33199.

<sup>3</sup> Department of Physics and Astronomy, Open University, Milton Keynes MK7 6AA, UK.

<sup>4</sup> Corresponding author; kaiser@gold.chem.hawaii.edu.

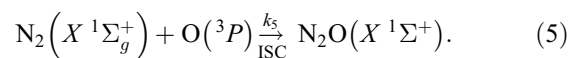
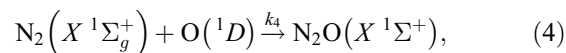
<sup>5</sup> See <http://www.ph1.uni-koeln.de/vorhersagen>.

region, where nitrous oxide has been identified. The third reaction is likely, since the reactants are known to be more abundant interstellar molecules. The rate of reaction ( $k_3$ ) is highly temperature dependent, and the reaction only becomes significant for temperatures above 125 K, where the rate  $k_3$  becomes larger than  $10^{-11}$  cm<sup>3</sup> s<sup>-1</sup>. Even though both reactants have been detected in the ISM, to arrive at the product from molecular nitrogen requires at least a two-step mechanism. For example, the first step may be the dissociation of molecular nitrogen and a hydroxyl radical by cosmic-ray bombardment followed by a reaction between the atoms to give nitric oxide and imidogen. The second step, as shown above (eq. [3]), is the reaction of nitric oxide and imidogen to give nitrous oxide and a hydrogen atom. However, multistep gas-phase reactions would give a low yield of the product in regions in which bimolecular reactions dominate, such as in the vacuum of interstellar space (Kaiser 2002). This is due to low collision rates and consequently long times between reactions on the way to forming the product. In addition, most interstellar environments such as cold molecular clouds do not have high enough temperatures to allow the above reaction to proceed to a substantial degree. Therefore, in order to accurately predict chemical abundances of nitrous oxide in the interstellar medium, solid-state reactions associated with grain chemistry must be included (Herbst 2002).

A more efficient mechanism of forming nitrous oxide in low-temperature environments like the interstellar medium (10 K) or in ices on Triton and Pluto (38 and 40 K, respectively; Tryka et al. 1993, 1994) would be solid-state neutral-neutral reactions, where one of the reactants would be either suprathermal (high kinetic energy) or electronically excited. This nonequilibrium chemistry can be initiated via energetic charged particles or through photodissociation processes. For example, in Saturn's magnetosphere a substantial fraction of the plasma is composed of N<sup>+</sup> (10%; Delitsky & Lane 2002). These ions incident on a water ice surface could react to give the nitrous oxide product. This reaction has relevance to the icy satellites of the Saturnian and Neptune systems, but since nitrogen ions are not abundant in the interstellar medium or near the surface of Pluto, this reaction may not prove to be significant in these environments.

An alternative chemical pathway involves the reaction of oxygen atoms with solid nitrogen. Note that the primary component of interstellar dust grains is water (Gibb et al. 2004). As MeV cosmic rays bombard these ice-coated interstellar grain particles, either suprathermal oxygen atoms [*O*(<sup>3</sup>*P*)] or oxygen atoms in the first electronically excited state [*O*(<sup>1</sup>*D*)] can be produced. In order to understand the reaction mechanism of how nitrous oxide and other molecules are formed, it is necessary to investigate reaction pathways for both the electronic ground state and excited states. For example, if it is determined that only ground-state atoms or molecules are responsible for reaction, then that would much simplify the possible reaction pathways to consider; however, excited-state chemistry has not been ruled out and may in fact contribute greatly (in combination with ground-state chemistry). This would open up other pathways that must be included in the astrochemical reaction models, since reactions with certain energy barriers at 10 K would no longer be insurmountable. In the production of nitrous oxide, an electronically excited oxygen atom could add to a neutral nitrogen molecule in a barrierless reaction to form nitrous oxide (reaction [4]), whereas the suprathermal oxygen atom could pass a conical intersection point (the energetically degenerate point at which two potential energy surfaces [PESs] of a polyatomic molecule overlap and thus intersystem crossing

[ISC] can occur) that lies 97 kJ mol<sup>-1</sup> above the energy of the separated reactants to reach the same product (Hwang & Mebel 2000; reaction [5]):



This could be a valid pathway for the formation of nitrous oxide on interstellar grains and in ices on Pluto and Triton. The low temperatures of these environments (10–40 K) will not prohibit the reaction, since excess energy, either in electronic or translational form, is given to the atomic oxygen reactant to induce nonequilibrium chemistry (Kaiser 2002). Nitrous oxide should, therefore, be expected to be produced wherever there exist molecular nitrogen ice, an oxygen-bearing component such as water, carbon monoxide, or carbon dioxide, and an irradiation source strong enough to liberate an oxygen atom to initiate non-equilibrium chemistry.

In this paper we investigate this hypothesis and untangle the formation of nitrous oxide by irradiating a homogeneously mixed ice layer of molecular nitrogen (N<sub>2</sub>) and carbon dioxide (CO<sub>2</sub>) at a ratio of 1:1 with 5 keV electrons. Several other previous papers have been published in which the authors have detected the nitrous oxide product by irradiation of an ice mixture. For example, Hudson & Moore (2002) identified nitrous oxide after irradiating a nitrogen–carbon dioxide ice mixture with 0.8 MeV protons. Other studies have found nitrous oxide using a variety of different ice mixtures and various irradiation sources that represent energetically unique environments of space. For example, keV ions can simulate the solar wind, ions in magnetospheres, or low-energy Galactic cosmic-ray ions (Benit et al. 1988; Strazzulla et al. 2001; Baratta et al. 2003), MeV protons represent the energetic distribution maximum of Galactic cosmic-ray ions (Moore et al. 1983; Hudson & Moore 2002), and ultraviolet radiation simulates the Galactic cosmic-ray radiation that permeates the Galaxy or the energetic electromagnetic radiation of a sun within a solar system (d'Hendecourt et al. 1986; Elsila et al. 1997). However, mechanistic and kinetic studies for the production of nitrous oxide as well the chemical processing effects due to electron irradiation have not been investigated.

In an earlier paper we demonstrated that the electrons actually simulate the  $\delta$ -electrons in the ultra track resulting from the primary processing of ices by MeV cosmic-ray particles (Bennett et al. 2004). Here, as an ion penetrates the ice it can lose energy by interacting with either the electronic or the nuclear potential of the target molecules. At the flux distribution maximum of the kinetic energy of Galactic cosmic-ray particles of about 10 MeV, 99.99% of the energy transferred from the cosmic-ray ion to the ices is released via electronic interaction. This leads to vibrational and/or electronic excitation of the target molecules. If given enough energy from the cosmic-ray ion, the molecule can also be ionized, releasing a so-called  $\delta$ -electron that leaves the molecule perpendicularly to the path of the cosmic-ray ion. Each  $\delta$ -electron, typically a few keV in energy, can chemically process molecules along its path by causing vibrational and/or electronic excitation as well as ionization; ultimately, these processes can lead to bond ruptures. One MeV cosmic-ray ion can interact with multiple molecules along its path, thereby creating a cascade of energetic  $\delta$ -electrons before the ion passes through the ice grain.

The nitrous oxide molecule was observed in our experiment, and it is our intent to understand the reaction pathway(s) and dynamics followed to arrive at the nitrous oxide product and to

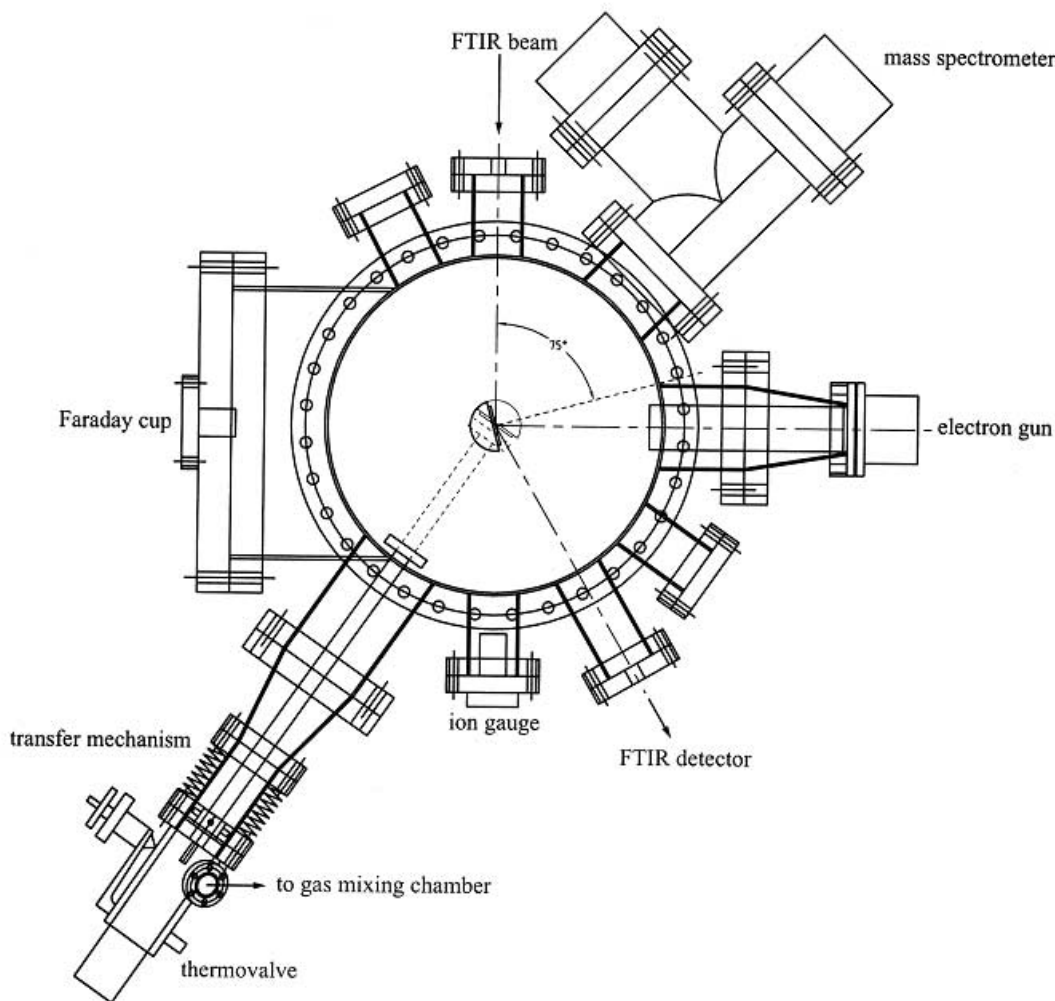


Fig. 1.—Top view of the experimental setup.

recognize the implications for the detection of nitrous oxide in the ISM and on the surfaces of solar system bodies.

## 2. EXPERIMENTAL

The experiment was carried out in a contamination-free ultrahigh vacuum (UHV) stainless steel chamber (see Fig. 1; Bennett et al. 2004). The chamber can reach pressures down to  $8 \times 10^{-11}$  torr by use of a magnetically suspended turbo molecular pump (TMP) that is backed by a scroll pump. All pumps used are oil-free to ensure that no hydrocarbon contaminants enter the system. Temperatures of 10 K are obtained using a two-stage closed-cycle helium refrigerator that is interfaced directly to a polished single-crystal silver mirror, onto which the ices are condensed. The silver substrate is suspended by a differentially pumped rotatable feedthrough, which aligns the wafer in the center of the main chamber. Gas condensation is carried out at 10 K, where the pressure is regulated by a Balzers UDV 235 thermovalve that lets gas through the linear transfer mechanism and to the gas capillary array (GCA), which evenly disperses the gas. The GCA can approach to within 5 mm of the mirror during condensation.

For this experiment, a molecular nitrogen ( $N_2$ )–carbon dioxide ( $CO_2$ ) ice mixture (1:1) was used. The gas mixture (146 and 54 mbar, respectively) was condensed for 5 minutes at a pressure of  $1.1 \times 10^{-7}$  torr at 10 K; note that because of the

fractionated condensation (molecules high in molecular weight and polarity have a greater probability of sticking to the substrate) of carbon dioxide, it is necessary to use a nitrogen-rich binary gas mixture so that a ratio of 1:1 can be reached in the ice sample. The unirradiated spectrum was recorded (Fig. 2) using a Nicolet 510 DX Fourier transform infrared (FTIR) spectrometer. Band assignments are given in Table 1. The spectrometer has a wavelength range of  $6000\text{--}500\text{ cm}^{-1}$  and operates in

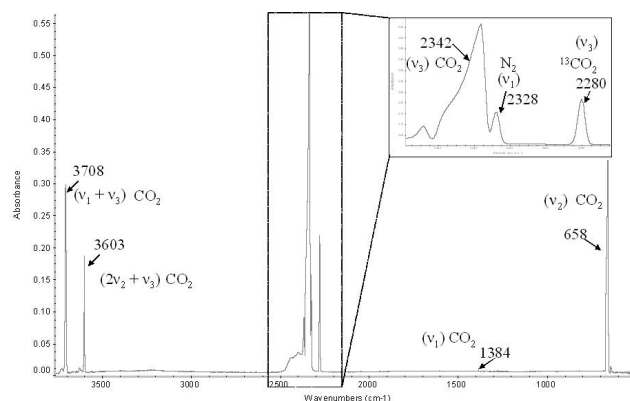


Fig. 2.—Infrared spectrum ( $3750\text{--}500\text{ cm}^{-1}$ ) of the nitrogen–carbon dioxide ice at 10 K before the irradiation.

TABLE 1  
INFRARED ABSORPTION FREQUENCY ASSIGNMENTS  
FOR THE NITROGEN-CARBON DIOXIDE ICE

Frequency (cm <sup>-1</sup> )	Assignment
3708.....	CO <sub>2</sub> (ν <sub>1</sub> + ν <sub>3</sub> )
3603.....	CO <sub>2</sub> (2ν <sub>2</sub> + ν <sub>3</sub> )
2342.....	CO <sub>2</sub> (ν <sub>3</sub> )
2328.....	N <sub>2</sub> (ν <sub>1</sub> )
2280.....	<sup>13</sup> CO <sub>2</sub> (ν <sub>3</sub> )
1384.....	CO <sub>2</sub> (ν <sub>1</sub> )
658.....	CO <sub>2</sub> (ν <sub>2</sub> )

absorption-reflection-absorption mode with a reflection angle of 75° from the normal relative to the mirror surface. Column densities of a molecule can be calculated according to Bennett et al. (2004). The calculated column densities were (4.5 ± 0.5) × 10<sup>17</sup> and (4.8 ± 0.5) × 10<sup>17</sup> molecules cm<sup>-2</sup> for nitrogen and carbon dioxide, respectively. Using the calculated column densities, the molecular weights, 28 and 44 g mol<sup>-1</sup>, and the densities, 1.03 (Scott 1976) and 1.7 g cm<sup>-3</sup> (Klinger et al. 1985), the respective thicknesses for molecular nitrogen (202 nm) and carbon dioxide (207 nm) ices were calculated.

The ice was irradiated isothermally with 5 keV electrons to simulate the δ-electrons resulting from cosmic-ray ion bombardment of an extraterrestrial ice. In our sample, each implanted electron transfers 2.6 keV to the solid (§ 4.3); this yields an averaged linear energy transfer (LET) of 6.4 ± 0.3 keV μm<sup>-1</sup>, i.e., a similar linear energy transfer to that of the 10 MeV protons [the distribution maximum LET(10 MeV H<sup>+</sup>) = 6.9 ± 0.2 keV μm<sup>-1</sup>] from the Galactic cosmic radiation field to the ice. This result is not surprising, as 99.99% of the energy transfer from the 10 MeV protons to the target molecules is used to generate δ-electrons. The electron beam was actually operated at a nominal current of 100 nA with an extraction efficiency of 78.8% and scanned over the sample area (3.0 ± 0.4 cm<sup>2</sup>) to avoid heating the ice. The sample was irradiated for 1 hr, which exposed the target to 1.8 × 10<sup>15</sup> electrons; longer irradiation times and higher beam currents should be avoided to eliminate overlapping electron trajectories and heating the ice surface (Bennett et al. 2004). The infrared spectra of the ice were recorded on line and in situ at an integrated time of 2.5 minutes and at a resolution of 2 cm<sup>-1</sup>. Our conditions simulate a processing of ice samples by the

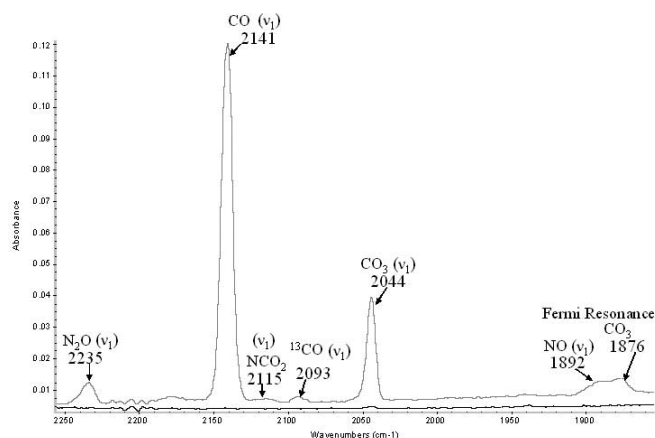


FIG. 3.—Infrared spectrum of the ice (2250–1850 cm<sup>-1</sup>) 1 hr after the irradiation (gray) against the unirradiated spectrum (black).

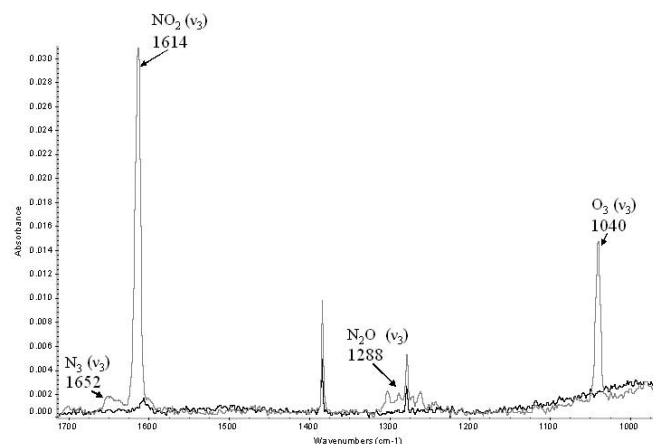


FIG. 4.—Infrared spectrum of the ice (1700–1000 cm<sup>-1</sup>) 1 hr after the irradiation (gray) against the unirradiated spectrum (black).

isotropic Galactic cosmic radiation field holding a flux distribution maximum of 10 cm<sup>-2</sup> s<sup>-1</sup> for 10 MeV H<sup>+</sup> and a duration of 5 × 10<sup>6</sup> yr.

### 3. RESULTS

The effects of the electron bombardment on the ice sample can be seen spectroscopically in Figures 3 and 4, and the observed species are presented in Table 2. The FTIR spectra are analyzed

TABLE 2  
INFRARED ABSORPTION FREQUENCIES OF NEW PEAKS DETECTED  
AFTER IRRADIATION AND THEIR ASSIGNMENTS

Frequency (cm <sup>-1</sup> )	Assignment
2235.....	(ν <sub>1</sub> ) N <sub>2</sub> O
2141.....	(ν <sub>1</sub> ) CO
2115.....	(ν <sub>1</sub> ) NCO <sub>2</sub>
2093.....	(ν <sub>1</sub> ) <sup>13</sup> CO
2044.....	(ν <sub>1</sub> ) CO <sub>3</sub>
1990 (tent.).....	(ν <sub>1</sub> ) C <sub>2</sub> O
1939 (tent.).....	(ν <sub>3</sub> ) OCN
1892.....	(ν <sub>1</sub> ) NO
1876.....	(Fermi res.) CO <sub>3</sub>
1854.....	(ν <sub>1</sub> ) c-N <sub>2</sub> O <sub>2</sub> (ν <sub>1</sub> ) t-N <sub>2</sub> O <sub>2</sub> (ν <sub>1</sub> ) asym-N <sub>2</sub> O <sub>4</sub>
1836.....	(ν <sub>1</sub> ) asym-N <sub>2</sub> O <sub>3</sub>
1764.....	(ν <sub>5</sub> ) c-N <sub>2</sub> O <sub>2</sub> (ν <sub>9</sub> ) sym-N <sub>2</sub> O <sub>4</sub>
1740.....	(ν <sub>5</sub> ) t-N <sub>2</sub> O <sub>2</sub> (ν <sub>1</sub> ) N <sub>2</sub> O <sub>5</sub> (ν <sub>9</sub> ) N <sub>2</sub> O <sub>5</sub>
1702.....	(ν <sub>3</sub> ) N <sub>3</sub> (ν <sub>2</sub> ) asym-N <sub>2</sub> O <sub>3</sub>
1652.....	(ν <sub>2</sub> ) asym-N <sub>2</sub> O <sub>4</sub>
1628.....	(ν <sub>3</sub> ) NO <sub>2</sub>
1614.....	(ν <sub>3</sub> ) NO <sub>3</sub>
1471.....	(ν <sub>1</sub> ) asym-N <sub>2</sub> O <sub>3</sub>
1303.....	(ν <sub>3</sub> ) asym-N <sub>2</sub> O <sub>4</sub> (ν <sub>2</sub> ) N <sub>2</sub> O <sub>5</sub> (ν <sub>1</sub> ) N <sub>2</sub> O
1288.....	(ν <sub>11</sub> ) sym-N <sub>2</sub> O <sub>4</sub>
1262.....	(ν <sub>10</sub> ) N <sub>2</sub> O <sub>5</sub>
1243.....	(ν <sub>2</sub> ) CO <sub>3</sub>
1067.....	(ν <sub>3</sub> ) O <sub>3</sub>
1040.....	(ν <sub>5</sub> ) CO <sub>3</sub>
978.....	

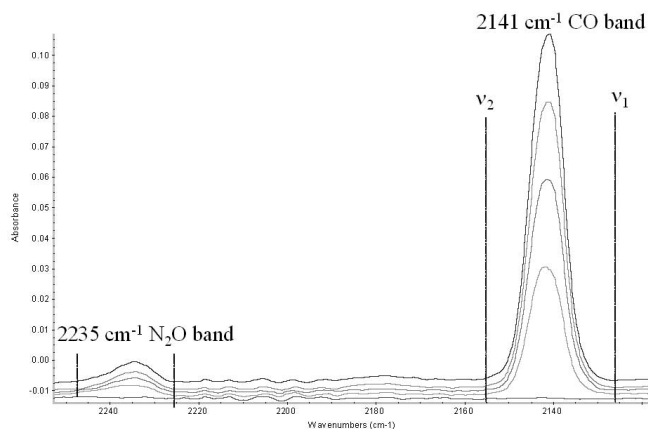


FIG. 5.—Temporal evolution of an absorption feature during the irradiation. Column densities  $n$  were calculated using band integrations according to Bennett et al. (2004).

in three steps. First, we investigate the new absorptions qualitatively and assign their carriers. Then, the temporal developments of these absorptions upon electron irradiation are investigated quantitatively (see Fig. 5). Finally, these data are fitted to kinetic rate laws to calculate production rates of synthesized molecules in units of molecules  $\text{cm}^{-2}$  (column density) and rate constants with units of  $\text{s}^{-1}$ . In order to calculate the column densities, the integral absorption coefficients were used for various bands of molecules observed in this experiment; these values are shown in Table 3. Solid-state absorption coefficients were used when available (for  $\text{CO}_2$ ,  $\text{CO}$ , and  $\text{N}_2$ ), but there have been no published coefficients or the validity of the value is questionable because of indirect means of calculation for the majority of the molecules ( $\text{O}_3$ ,  $\text{CO}_3$ ,  $\text{NCO}_2$ ,  $\text{N}_3$ , and the  $\text{N}_x\text{O}_y$  species). In these cases, gas-phase and/or theoretical calculations were used; these can differ up to 20%–30% from the actual solid-state value. The integration routine of the absorption features is accurate to  $\pm 10\%$  (Kaiser et al. 1995).

### 3.1. Qualitative Analysis

In comparing the infrared spectrum of the ice before and after irradiation, it is apparent that additional peaks exist after the exposure of the target to the electron irradiation (Table 2). Many of the products observed can result from irradiation of the pure ices, as shown by Gerakines et al. (1996), but there are also other products that must result from irradiation of the nitrogen and carbon dioxide van der Waals complexes. The most intense absorption seen after irradiation is the  $2141 \text{ cm}^{-1}$  band, which has been assigned to the  $\nu_1$  stretching vibration of the carbon monoxide molecule ( $\text{CO}$ ). This product is expected to be produced in high quantities, since carbon monoxide results from the primary dissociation pathway of carbon dioxide during electron irradiation, which also produces ground-state ( $^3P$ ) and electronically excited oxygen atoms ( $^1D$ ; Bennett et al. 2004). The isotope of carbon monoxide ( $^{13}\text{CO}$ ) was also detected at  $2093 \text{ cm}^{-1}$ . Four absorptions of the cyclic,  $\text{C}_{2v}$  symmetric carbon trioxide molecule were found at  $2044 \text{ cm}^{-1}$  ( $\nu_1$ ),  $1876 \text{ cm}^{-1}$ , which is thought to be a Fermi resonance of the  $\nu_1$  band with an overtone of the  $973 \text{ cm}^{-1}$  fundamental, and  $1067$  ( $\nu_2$ ). A tentative absorption can be seen at  $978 \text{ cm}^{-1}$ , which matches the expected  $\nu_5$  fundamental of  $973 \text{ cm}^{-1}$ . These results are in good agreement with the previous studies investigating the carbon trioxide molecule (Moll et al. 1966; Jacox & Milligan 1971; Bennett et al. 2004). An intense absorption due to bent ozone

TABLE 3  
ABSORPTION COEFFICIENTS USED IN COLUMN DENSITY CALCULATIONS  
FOR THE OBSERVED MOLECULES

Absorption Band ( $\text{cm}^{-1}$ )	Absorption Coefficient ( $\text{cm molecule}^{-1}$ )	Reference
3708 ( $\text{CO}_2$ ).....	1.40E–18	1
3603 ( $\text{CO}_2$ ).....	4.50E–19	1
2328 ( $\text{N}_2$ ).....	3.00E–19	2
2235 ( $\text{N}_2\text{O}$ ).....	5.20E–17	3
2141 ( $\text{CO}$ ).....	1.10E–17	1
2115 ( $\text{NCO}_2$ ).....	8.50E–17	4
2044 ( $\text{CO}_3$ ).....	8.90E–17	5
1892 ( $\text{NO}$ ).....	6.81E–18	6
1876 ( $\text{CO}_3$ ).....	3.10E–17	5
1836 (asym- $\text{N}_2\text{O}_3$ ).....	6.43E–17	6
1764 (c- $\text{N}_2\text{O}_2$ ).....	1.50E–16	6
1740 (t- $\text{N}_2\text{O}_2$ ).....	2.72E–17	7
1702 ( $\text{N}_2\text{O}_5$ ).....	3.80E–17	6
1652 ( $\text{N}_3$ ).....	4.00E–17	8
1652 (asym- $\text{N}_2\text{O}_3$ ).....	6.24E–17	6
1628 (asym- $\text{N}_2\text{O}_4$ ).....	5.95E–17	6
1614 ( $\text{NO}_2$ ).....	6.36E–17	6
1471 ( $\text{NO}_3$ ).....	7.64E–18	6
1303 (asym- $\text{N}_2\text{O}_3$ ).....	4.63E–17	6
1303 (asym- $\text{N}_2\text{O}_4$ ).....	5.60E–17	6
1303 ( $\text{N}_2\text{O}_5$ ).....	7.00E–18	6
1262 (sym- $\text{N}_2\text{O}_4$ ).....	8.50E–17	6
1243 ( $\text{N}_2\text{O}_5$ ).....	7.40E–17	6
1040 ( $\text{O}_3$ ).....	1.40E–17	9

REFERENCES.—(1) Gerakines et al. 1995; (2) Bernstein & Sandford 1999; (3) Wang et al. 2001; (4) Benson & Francisco 1995; (5) Bennett et al. 2004; (6) Stürling et al. 1994; (7) Krim 1998; (8) this work; (9) Smith et al. 1985.

( $\text{O}_3$ ) was observed at  $1040 \text{ cm}^{-1}$  ( $\nu_3$ , antisymmetric stretch). This assignment was confirmed by previous work (Shimanouchi 1977; Bennett et al. 2004).

Nitrous oxide ( $\text{N}_2\text{O}$ ) was positively identified by the NN stretch at  $2235 \text{ cm}^{-1}$  (Sodeau & Withnall 1985). A confirmation band of the NO stretch at  $1288 \text{ cm}^{-1}$  is tentatively assigned; however, other absorptions in that region prohibit matching the slopes of the temporal traces for the two nitrous oxide bands to confirm the  $1288 \text{ cm}^{-1}$  feature. The band assignments correlate with the linear structure. For comparison, vibrational frequency calculations were carried out at the B3LYP/6-311G(d) level of theory to investigate the formation of the cyclic nitrous oxide isomer (Hwang & Mebel 2000). The experimental values correspond well to the theoretical calculations after acknowledging that the vibrations occur in different media (Table 4). No identification for the cyclic nitrous oxide isomer at  $744 \text{ cm}^{-1}$  could be made, possibly because the calculated intensity of the strongest absorption band is 30 times weaker compared to the linear structure. Note that the  $607 \text{ cm}^{-1}$  band of the linear nitrous oxide molecule could not be identified either; this feature holds approximately the same intensity as the most intense  $744 \text{ cm}^{-1}$  band from the unobserved cyclic nitrous oxide isomer.

We would like to stress that additional peaks were observed, including assignments for  $\text{NCO}_2$  ( $2115 \text{ cm}^{-1}$ ),  $\text{NO}$  ( $1892 \text{ cm}^{-1}$ ), asym- $\text{N}_2\text{O}_3$  ( $1836 \text{ cm}^{-1}$ ), cis- $\text{N}_2\text{O}_2$  ( $1764 \text{ cm}^{-1}$ ), trans- $\text{N}_2\text{O}_2$  ( $1740 \text{ cm}^{-1}$ ),  $\text{NO}_3$  ( $1471 \text{ cm}^{-1}$ ),  $\text{N}_2\text{O}_5$  ( $1702 \text{ cm}^{-1}$ ),  $\text{N}_3$  ( $1652 \text{ cm}^{-1}$ ), asym- $\text{N}_2\text{O}_4$  ( $1628 \text{ cm}^{-1}$ ),  $\text{NO}_2$  ( $1614 \text{ cm}^{-1}$ ), and sym- $\text{N}_2\text{O}_4$  ( $1262 \text{ cm}^{-1}$ ). An analysis of the complete kinetics of these species will be presented in a forthcoming article; their presence has no effect on the mechanistic determination of the formation of nitrous oxide as presented in this paper.

TABLE 4  
CALCULATED HARMONIC INFRARED ABSORPTION FREQUENCIES OF THE LINEAR AND THE CYCLIC NITROUS OXIDE MOLECULES COMPARED WITH EXPERIMENTALLY OBSERVED FREQUENCIES

EXPERIMENTALLY OBSERVED FREQUENCY ( $\text{cm}^{-1}$ )	LINEAR $\text{N}_2\text{O}$		CYCLIC $\text{N}_2\text{O}$	
	Calculated Frequency ( $\text{cm}^{-1}$ )	Intensity ( $\text{km mol}^{-1}$ )	Calculated Frequency ( $\text{cm}^{-1}$ )	Intensity ( $\text{km mol}^{-1}$ )
2235.....	2283	348.8	1858	1.7
1288.....	1296	56.2	744	11.3
	607	8.1	351	3.6

NOTE.—The calculated frequencies have been scaled by a factor of 0.97 to account for anharmonicities.

### 3.2. Quantitative Analysis

#### 3.2.1. Carbon Balance

The temporal development of the column densities of the carbon dioxide reactant and of products relevant to elucidating the formation of the nitrous oxide species (carbon monoxide, carbon trioxide, ozone, and nitrous oxide) are summarized in Figures 6–11. As expected, during the irradiation of the carbon dioxide ice, the column density of the  $\text{CO}_2$  molecule decreases only slightly by  $(3.5 \pm 0.5) \times 10^{16} \text{ cm}^{-2}$  from  $(5.5 \pm 1.4) \times 10^{17} \text{ cm}^{-2}$  (Figs. 6 and 7) during the 1 hr irradiation period; we averaged the data for two absorption bands at 3708 and 3603  $\text{cm}^{-1}$ . Therefore, only  $6\% \pm 2\%$  of the carbon dioxide molecules are being destroyed during the irradiation. Accounting for the target surface and the electron beam current, we calculate that each implanted electron degrades  $58 \pm 18$  carbon dioxide molecules.

As the carbon dioxide column density decreases, additional absorptions appear from carbon monoxide (Fig. 8) and carbon trioxide (Fig. 9). The carbon monoxide column density increases to  $(2.8 \pm 0.5) \times 10^{16} \text{ cm}^{-2}$ , i.e., an average production rate of  $47 \pm 5$  carbon monoxide molecules per implanted electron. The carbon trioxide column density rises quickly and saturates after about 30 minutes of irradiation; at the end of the experiment  $(0.9 \pm 0.1) \times 10^{15}$  molecules  $\text{cm}^{-2}$  are formed. This suggests a production rate of  $1.5 \pm 0.5$  carbon trioxide molecules per electron. Note that  $(9.6 \pm 0.9) \times 10^{15}$   $\text{NCO}_2$  molecules  $\text{cm}^{-2}$  were synthesized as well ( $16 \pm 2$   $\text{NCO}_2$  molecules per implant). These data help us to cross-check the carbon balance of

the target. Here the destruction of  $58 \pm 18$  carbon dioxide molecules, either via degradation or reaction, per implanted electron leads to the formation of  $47 \pm 5$  carbon monoxide,  $1.5 \pm 0.5$  carbon trioxide, and  $16 \pm 2$   $\text{NCO}_2$  molecules, i.e., a production of  $64.5 \pm 7.5$  carbon-bearing species. This suggests that within the error limits, the carbon budget is conserved inside the ice target.

#### 3.2.2. Oxygen Balance

It is also important to investigate the oxygen balance of the target. Since the primary dissociation pathway of the carbon dioxide molecule is the formation of an oxygen atom plus carbon monoxide (Bennett et al. 2004), the number of synthesized carbon monoxide species is equivalent to the number of released oxygen atoms, i.e.,  $47 \pm 5$  per implanted electron. Which oxygen-bearing species are formed during the irradiation exposure? These are the carbon trioxide species ( $1.5 \pm 0.5$  per implant; see § 3.2.1), the ozone molecule ( $3.5 \pm 0.5$  per electron), which accounts for  $10.5 \pm 1.5$  of the bonded oxygen atoms per implanted electron, and the newly formed nitrous oxide molecule (Fig. 10). For nitrous oxide, the column density rises to  $(3.2 \pm 0.3) \times 10^{14} \text{ cm}^{-2}$ , i.e., an average formation of  $0.5 \pm 0.1$  nitrous oxide molecules per implant. Adding these species brings us to  $12.5 \pm 2.1$  accounted oxygen atoms per electron versus a production rate of  $47 \pm 5$  atoms per implant. What is the fate of the missing oxygen atoms? We have to consider that besides those species relevant to explaining the formation route of nitrous oxide in low-temperature ices, we are also synthesizing higher order reaction products such as nitric

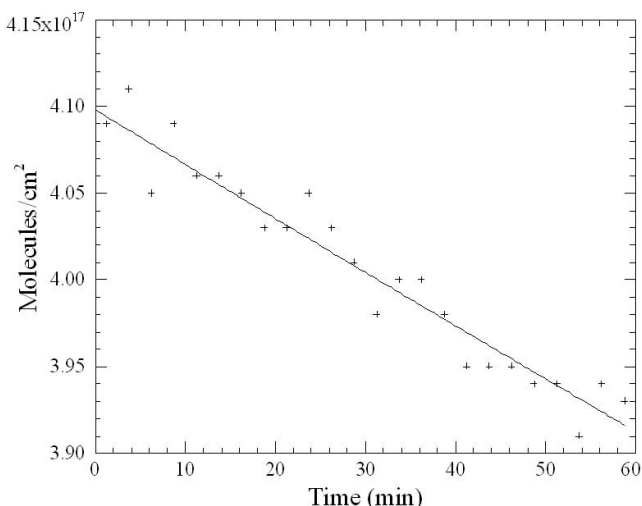


FIG. 6.—Temporal profile of the 3708  $\text{cm}^{-1}$  absorption feature of  $\text{CO}_2$  throughout the irradiation. Error bars of 10% have been omitted for clarity.

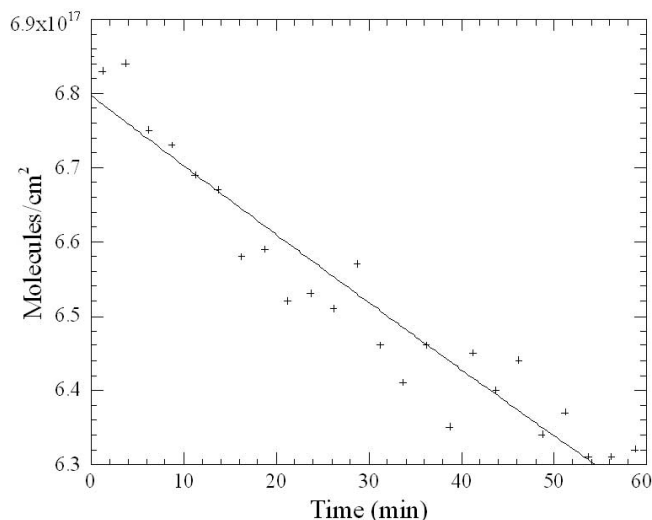


FIG. 7.—Temporal profile of the 3603  $\text{cm}^{-1}$  absorption feature of  $\text{CO}_2$  throughout the irradiation. Error bars of 10% have been omitted for clarity.

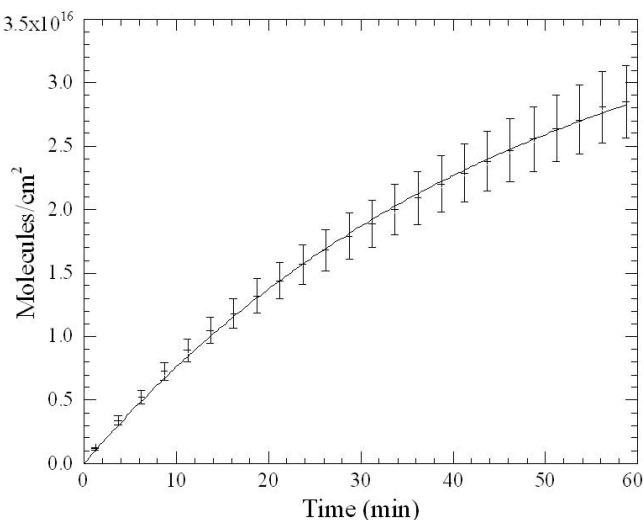


FIG. 8.—Temporal profile of the  $2141\text{ cm}^{-1}$  absorption feature of CO throughout the irradiation.

oxide  $[(6.9 \pm 0.7) \times 10^{15}\text{ NO cm}^{-2}]$ , nitrogen dioxide  $[(1.2 \pm 0.1) \times 10^{15}\text{ NO}_2\text{ cm}^{-2}]$ , cis and trans dinitrogen dioxide  $[(1.9 \pm 0.2) \times 10^{13}$  and  $(2.6 \pm 0.3) \times 10^{13}\text{ N}_2\text{O}_2\text{ cm}^{-2}]$ , nitrogen trioxide  $[(3.0 \pm 0.3) \times 10^{14}\text{ NO}_3\text{ cm}^{-2}]$ , asymmetric dinitrogen trioxide  $[(4.9 \pm 0.5) \times 10^{13}\text{ N}_2\text{O}_3\text{ cm}^{-2}]$ , sym and asym dinitrogen tetroxide  $[(3.8 \pm 0.4) \times 10^{13}$  and  $(4.1 \pm 0.4) \times 10^{13}\text{ N}_2\text{O}_4\text{ cm}^{-2}]$ , and dinitrogen pentoxide  $[(4.6 \pm 0.5) \times 10^{13}\text{ N}_2\text{O}_5\text{ cm}^{-2}]$ . Although this increases the number of accounted oxygen atoms to  $30 \pm 3$  per implant, this number still falls short of correlating with the predicted value of  $47 \pm 5$  by about  $36\% \pm 6\%$ . However, thus far we have only reported those species that are infrared active. In neat carbon dioxide systems, the formation of ozone proceeds through a stepwise mechanism via reaction of two oxygen atoms forming the infrared-inactive oxygen molecule, followed by reaction of the latter with a third oxygen atom (Bennett et al. 2004). Therefore, we can also suggest that the carbon dioxide–nitrogen ice still stores reactive ground-state oxygen atoms and infrared-inactive molecular oxygen that could account for the missing balance of oxygen atoms (see § 4.1).

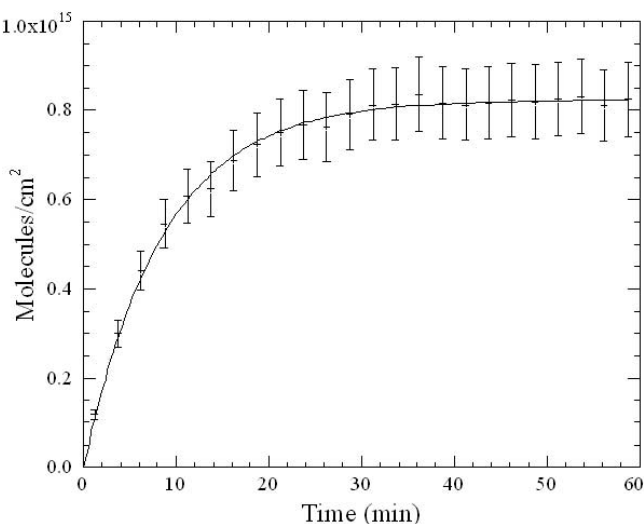


FIG. 9.—Temporal profile of the  $2044\text{ cm}^{-1}$  absorption feature of  $\text{CO}_3$  throughout the irradiation.

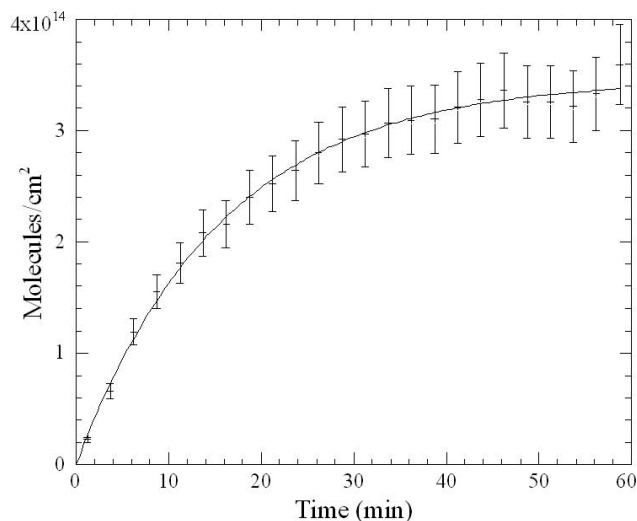


FIG. 10.—Temporal profile of the  $2235\text{ cm}^{-1}$  absorption feature of  $\text{N}_2\text{O}$  throughout the irradiation.

### 3.2.3. Nitrogen Balance

Finally, we would like to briefly address the nitrogen balance of the target. During the irradiation of the target, the column density of molecular nitrogen decreases by  $(3.7 \pm 0.5) \times 10^{16}\text{ cm}^{-2}$ . This is due to reaction of the nitrogen molecule with other components, including molecular oxygen, to yield nitrous oxide (§ 3.1) and the formation of two nitrogen atoms per dissociated nitrogen molecule; therefore we have to account for  $(7.4 \pm 1.0) \times 10^{16}\text{ N atoms cm}^{-2}$ . To verify the nitrogen balance, we first add the column densities of the nitrogen atoms as found in nitrous oxide  $[(3.2 \pm 0.3) \times 10^{14}\text{ N}_2\text{O cm}^{-2}]$ , cyanocarbonyl  $[(9.6 \pm 0.9) \times 10^{15}\text{ NCO cm}^{-2}]$ , nitric oxide  $[(6.9 \pm 0.7) \times 10^{15}\text{ NO cm}^{-2}]$ , nitrogen dioxide  $[(1.2 \pm 0.1) \times 10^{15}\text{ NO}_2\text{ cm}^{-2}]$ , cis and trans dinitrogen dioxide  $[(1.9 \pm 0.2) \times 10^{13}$  and  $(2.6 \pm 0.3) \times 10^{13}\text{ N}_2\text{O}_2\text{ cm}^{-2}]$ , nitrogen trioxide  $[(3.0 \pm 0.3) \times 10^{14}\text{ NO}_3\text{ cm}^{-2}]$ , asymmetric dinitrogen trioxide  $[(4.9 \pm 0.5) \times 10^{13}\text{ N}_2\text{O}_3\text{ cm}^{-2}]$ , sym and asym dinitrogen tetroxide  $[(3.8 \pm 0.4) \times 10^{13}$  and  $(4.1 \pm 0.4) \times 10^{13}\text{ N}_2\text{O}_4\text{ cm}^{-2}]$ , dinitrogen pentoxide  $[(4.6 \pm 0.5) \times 10^{13}\text{ N}_2\text{O}_5\text{ cm}^{-2}]$ , and the azide radical  $[(4.2 \pm 0.4) \times 10^{13}\text{ N}_3\text{ cm}^{-2}]$ . This

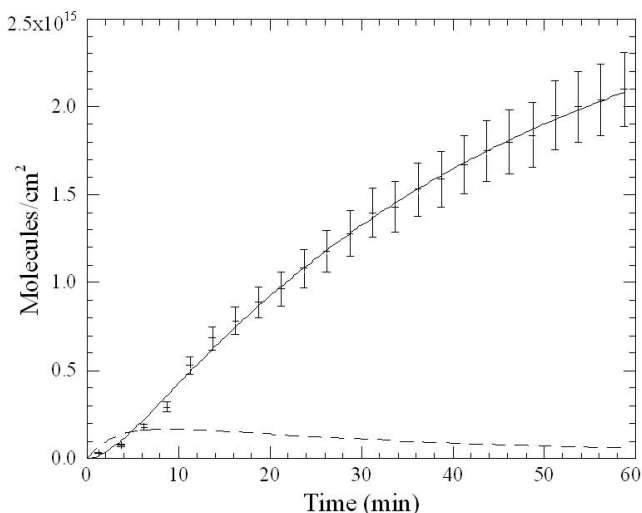


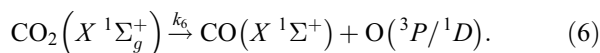
FIG. 11.—Temporal profile of the  $1040\text{ cm}^{-1}$  absorption feature of  $\text{O}_3$  throughout the irradiation (solid line). The dashed line represents the calculated evolution of the column density of molecular oxygen.

brings us to  $(1.9 \pm 0.3) \times 10^{16}$  N cm<sup>-2</sup> that are accounted for compared to  $(7.4 \pm 1.0) \times 10^{16}$  N cm<sup>-2</sup> as derived from the decay of the molecular nitrogen column density. The “missing” nitrogen atoms most likely exist as nitrogen atoms in the 10 K sample; this is similar to the existence of oxygen atoms, which can still be stored in the low-temperature ices after the electron irradiation (§ 3.2.2). Considering the sample area of 3 cm<sup>2</sup>,  $(1.6 \pm 0.3) \times 10^{17}$  nitrogen atoms are stored after the irradiation. Finally, we would like to investigate how many of the nitrogen molecules were actually destroyed by a chemical reaction or were dissociated to two nitrogen atoms by the electron irradiation. The data suggest that  $(7.4 \pm 0.9) \times 10^{16}$  cm<sup>-2</sup> nitrogen atoms were generated by dissociation of  $(3.7 \pm 0.5) \times 10^{16}$  N<sub>2</sub> molecules cm<sup>-2</sup>, i.e., a destruction of  $62 \pm 9$  nitrogen molecules per implanted electron; this is similar to the electron-induced degradation of  $47 \pm 5$  carbon dioxide molecules. Hence only  $8\% \pm 2\%$  of the nitrogen has been dissociated during the irradiation; this compares well with a  $6\% \pm 2\%$  degradation fraction of carbon dioxide.

#### 4. DISCUSSION

##### 4.1. Kinetics

To investigate the kinetics and dynamics of the formation of the nitrous oxide molecule, it is important to model the abundance of each molecule through time. Here the integrated absorbance for each species was calculated versus time throughout the irradiation, as depicted in Figure 5. The absorbance profiles together with the fits for those molecules relevant to understanding the synthesis of nitrous oxide in interstellar ices (carbon dioxide, carbon monoxide, carbon trioxide, nitrous oxide, and ozone) are shown in Figures 6–11. Our studies suggest that the response of the ice upon the keV electron bombardment is governed by an initial formation of carbon monoxide and atomic oxygen,



Here the electron-induced decomposition of carbon dioxide is endoergic by 532 kJ mol<sup>-1</sup> (5.51 eV) to form carbon monoxide and a ground-state oxygen atom on the triplet surface and endoergic by 732 kJ mol<sup>-1</sup> (7.59 eV) to generate carbon monoxide and an electronically excited oxygen atom on the singlet surface (Bennett et al. 2004). Abundances of both the carbon dioxide parent molecule and carbon monoxide product can be fitted following first-order kinetics. Here the rate of disappearance of carbon dioxide is

$$\frac{-d[\text{CO}_2]}{dt} = k_6[\text{CO}_2], \quad (7)$$

which leads to the temporal evolution for the column density of the carbon dioxide molecule,

$$[\text{CO}_2](t) = [\text{CO}_2](t=0) e^{-k_6 t} = a e^{-k_6 t}. \quad (8)$$

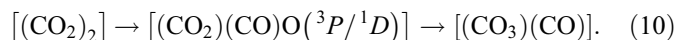
For carbon dioxide, a best-fit curve was produced for both the 3708 and 3603 cm<sup>-1</sup> bands (Figs. 6 and 7) to match the data, where  $a = (4.098 \pm 0.006) \times 10^{17}$  molecules cm<sup>-2</sup> and  $k_6 = (7.70 \pm 0.04) \times 10^{-4}$  s<sup>-1</sup> for the 3708 cm<sup>-1</sup> feature. For the 3603 cm<sup>-1</sup> band, we found best fits of  $a = (6.80 \pm 0.02) \times 10^{17}$  molecules cm<sup>-2</sup> and  $k_6 = (1.40 \pm 0.08) \times 10^{-3}$  s<sup>-1</sup>. The  $a$ -value is equivalent to the initial carbon dioxide column density, i.e.,  $5.5 \times 10^{17}$  molecules cm<sup>-2</sup> as averaged over both bands.

We would like to stress that the integrated absorption coefficients for the carbon dioxide were derived from transmission experiments, but the experiment has been carried out in an absorption-reflection-absorption mode. This probably causes the variation in the film thicknesses estimated from different absorption features. After irradiation, the abundance of carbon dioxide was observed to decrease (§ 3) by  $(3.5 \pm 0.5) \times 10^{16}$  cm<sup>-2</sup>, indicating that only  $6\% \pm 2\%$  of the carbon dioxide was destroyed either by the irradiation process or reacting to other products. Actually, the amount of carbon dioxide that dissociated upon electron irradiation can be calculated by looking at the production of the carbon monoxide species (Fig. 7). Here the temporal evolution of the integrated absorbance of the 2141 cm<sup>-1</sup> band from carbon monoxide can be fitted with a simple first-order rise via

$$[\text{CO}](t) = b(1 - e^{-k_7 t}). \quad (9)$$

We yielded best-fit values of  $b = (3.94 \pm 0.08) \times 10^{16}$  molecules cm<sup>-2</sup> and  $k_7 = (3.5 \pm 0.1) \times 10^{-4}$  s<sup>-1</sup>. Comparing the production of carbon monoxide to the disappearance of carbon dioxide, more carbon dioxide is destroyed than carbon monoxide is produced. This could be accounted for by realizing that carbon dioxide can actually react to form other species like carbon trioxide (CO<sub>3</sub>, *X*<sup>1</sup>A<sub>1</sub>) and the bent, C<sub>s</sub> symmetric nitrosocarbonyl radical (ONCO, *X*<sup>2</sup>A''), so that not all of the disappearing carbon dioxide produces carbon monoxide. In fact,  $81\% \pm 15\%$  of the carbon dioxide molecules were cleaved to form carbon monoxide and atomic oxygen via equation (6). The remaining carbon dioxide molecules reacted with oxygen and nitrogen atoms to the CO<sub>3</sub> ( $3\% \pm 1\%$ ) and the ONCO ( $27\% \pm 3\%$ ) species, respectively. The enhanced reactivity of the nitrogen atoms versus atomic oxygen with carbon dioxide is currently under investigation.

We now examine the kinetics of the carbon trioxide formation. It was found that the production of carbon trioxide follows pseudo-first-order kinetics. Formally, the mechanism involves a decomposing carbon dioxide van der Waals dimer; a fraction of the oxygen atoms that are released upon interaction of the electron with one carbon dioxide molecule reacts within the matrix cage with the second carbon dioxide molecule:

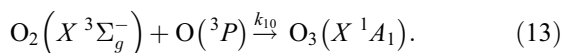
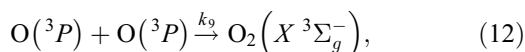


A full kinetics study for the formation of the cyclic carbon trioxide isomer in pure carbon dioxide ices is presented by Bennett et al. (2004). Assuming pseudo-first-order kinetics in the carbon dioxide–nitrogen ice, the temporal evolution of the column density of the carbon trioxide should follow

$$[\text{CO}_3](t) = c(1 - e^{-k_8 t}). \quad (11)$$

Fitting this equation to the temporal evolution of the integrated absorption feature (Fig. 9) yields  $c = (8.23 \pm 0.04) \times 10^{14}$  molecules cm<sup>-2</sup> and  $k_8 = (1.93 \pm 0.02) \times 10^{-3}$  s<sup>-1</sup>. Throughout the irradiation  $(2.8 \pm 0.5) \times 10^{16}$  molecules cm<sup>-2</sup> of carbon monoxide were produced, and, via equation (6), it is evident that the same number of oxygen atoms should be produced. By comparison with the abundance of carbon trioxide after the 1 hr of irradiation, it is calculated that only  $3\% \pm 1\%$  of the liberated oxygen atoms produced react with carbon dioxide to form carbon trioxide. This value compares well (it is within the error limits) with the value reported by Bennett et al. (2004) of  $4\% \pm 1\%$ .

Another observed product that resulted from the irradiation processing of carbon dioxide, as shown by Bennett et al. (2004) in the neat carbon dioxide system, was ozone. The temporal evolution of the ozone band is indicative of a higher order reaction product via



As seen in Figure 11, the curve shape does not fit a simple pseudo-first-order reaction, demonstrating that the formation of ozone does indeed follow higher order kinetics. Here we attempt to fit the data contemplating a reaction sequence of the type  $A \rightarrow B \rightarrow C$ , with A formally being equal to a carbon dioxide trimer,  $[(\text{CO}_2)_3]$ , that is to be decomposed by the electron irradiation, B, the  $[(\text{CO})_3\text{-O-O}_2]$  complex within the matrix emerging from the reaction of two liberated oxygen atoms via equation (12) in the matrix cage, and C, the ozone molecule formally observed in the  $[(\text{CO})_3\text{-O}_3]$  matrix cage. This results in a temporal dependence of the ozone column density of

$$[\text{O}_3](t) = f \left( 1 - \frac{k_{10}}{k_{10} - k_9} e^{-k_9 t} + \frac{k_9}{k_{10} - k_9} e^{-k_{10} t} \right). \quad (14)$$

According to the best-fit values,  $f = (2.9 \pm 0.1) \times 10^{15}$  molecules  $\text{cm}^{-2}$ ,  $k_9 = (3.8 \pm 0.3) \times 10^{-4}$   $\text{s}^{-1}$ , and  $k_{10} = (5.3 \pm 0.8) \times 10^{-3}$   $\text{s}^{-1}$ . This suggests that the formation of the ozone species ( $k_{10}$ ) is much faster than the formation of the oxygen molecule ( $k_9$ ) in the  $[(\text{CO})_3\text{-O-O}_2]$  complex, such that any molecular oxygen produced would quickly react to ozone. Most importantly, we can use  $k_9$ , i.e., the rate constant for the formation of oxygen, to calculate how many oxygen molecules were formed during the irradiation process (recall that we were unable to observe molecular oxygen spectroscopically, because this molecule is infrared inactive; Fig. 11). Using the rate constant  $k_9$ , we find that  $(5.7 \pm 0.6) \times 10^{13}$  molecules  $\text{cm}^{-2}$  were formed during the irradiation, i.e., a production of  $0.1 \pm 0.01$  oxygen molecules per implanted electron. This does not increase the number of accounted oxygen atoms significantly from  $30 \pm 3$  (§ 3.2.2); the remaining  $17 \pm 9$  missing oxygen atoms (per implant) must therefore exist in atomic form in their  $^3P$  electronic ground state after the irradiation has stopped.

Finally, we analyze the temporal profile of the integrated absorption of the  $2235 \text{ cm}^{-1}$  feature of nitrous oxide. Here the data also follow pseudo-first-order kinetics. This is a logical finding, since once an oxygen atom is produced by irradiation, it will react rapidly with a matrix molecule. The kinetics of nitrous oxide was investigated using the temporal evolution plot of the column density in Figure 10. In the calculations it was modeled that the production of nitrous oxide follows a first-order rate law via equations (15) and (16), formally via an electron-induced decomposition of a nitrogen-carbon dioxide van der Waals complex ( $\text{N}_2\text{-CO}_2$ ), followed by a reaction of the released oxygen atom with a nitrogen molecule in the matrix cage:

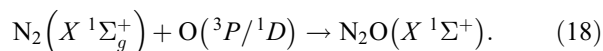
$$\frac{-d[\text{N}_2\text{-CO}_2]}{dt} = k_{11}[\text{N}_2\text{-CO}_2], \quad (15)$$

$$\frac{d[\text{N}_2\text{O}]}{dt} = k_{12}[\text{N}_2\text{-CO}_2]. \quad (16)$$

This then leads to the temporal dependence of the column density (Steinfeld et al. 1989), where the production of nitrous oxide follows

$$[\text{N}_2\text{O}](t) = d(1 - e^{-k_{12}t}). \quad (17)$$

The absorption coefficient of the  $2235 \text{ cm}^{-1}$  band was taken from Wang et al. (2001) to be  $5.2 \times 10^{-17}$   $\text{cm molecule}^{-1}$ . This procedure yields a best fit with  $d = (3.46 \pm 0.03) \times 10^{14}$  molecules  $\text{cm}^{-2}$  and  $k_{12} = (6.4 \pm 0.2) \times 10^{-2}$   $\text{s}^{-1}$ . The small sigma values relative to their respective constants indicate that it is justified to assume pseudo-first-order kinetics in the production of nitrous oxide. This allows for the identification of a mechanism that is first order to form nitrous oxide via



The oxygen atoms required for this reaction are supplied by the dissociation of carbon dioxide via irradiation through equation (6). Over the 1 hr of irradiation,  $(3.2 \pm 0.3) \times 10^{14}$  molecules  $\text{cm}^{-2}$  of linear nitrous oxide were produced.

#### 4.2. Dynamics

In § 4.1 we investigated the temporal evolution of the newly formed species and fitted the graphs with first and higher order reaction models. This yielded rate constants and production rates of carbon monoxide ( $k_7$ ), carbon trioxide ( $k_8$ ), molecular oxygen ( $k_9$ ), ozone ( $k_{10}$ ), and nitrous oxide ( $k_{12}$ ). Here we attempt to untangle the actual mechanism of how the nitrous oxide molecule is synthesized in low-temperature ices. This mechanism has to account for the fact that the reaction rate of the liberated oxygen atoms with carbon dioxide to form carbon trioxide [ $k_8 = (1.93 \pm 0.02) \times 10^{-3}$   $\text{s}^{-1}$ ] is lower than the competing reaction of oxygen atoms with molecular nitrogen to give the nitrous oxide molecule [ $k_{12} = (6.4 \pm 0.2) \times 10^{-2}$   $\text{s}^{-1}$ ] by a factor of  $33 \pm 1$ . On the other hand, that the actual column density of newly formed carbon trioxide [ $(9.0 \pm 1.0) \times 10^{14}$  molecules  $\text{cm}^{-2}$ ] is larger by a factor of  $2.8 \pm 0.6$  compared to the nitrous oxide molecules [ $(3.2 \pm 0.3) \times 10^{14}$  molecules  $\text{cm}^{-2}$ ].

The feasible reaction pathways of an oxygen atom reacting with molecular nitrogen are seen schematically on the PES presented in Figure 12. First, an electronically excited oxygen atom ( $^1D$ ) can add on the singlet surface to a nonbonding electron pair on one of the nitrogen atoms; this pathway is barrierless and leads to the nitrous oxide product. Ab initio calculations by Hwang & Mebel (2000) show that this reaction has an exoergicity of  $\Delta_r G^\circ = -370 \text{ kJ mol}^{-1}$  to the linear nitrous oxide structure. The negative Gibbs free energy of the reaction indicates that the process is spontaneous. Had the reaction been endoergic, the amount of energy available to the reactants would need to be compared to the energy difference between the products and the reactants to see whether the reaction could still proceed. The products are energetically lower than the reactants, so the reaction should occur regardless of the energy of the reactants (there being no entrance barrier). After reaction, the excess energy would be dissipated in the form of phonons in the ice matrix in order to energetically stabilize the product. An alternative route on the singlet surface is the addition of an electronically excited oxygen atom to the nitrogen-nitrogen triple bond of the nitrogen molecule. This pathway proceeds barrierlessly through a cyclic intermediate that lies  $100 \text{ kJ mol}^{-1}$  below the reactants. The cyclic structure ring opens via a transition state (TS1) to the product. The reaction can also

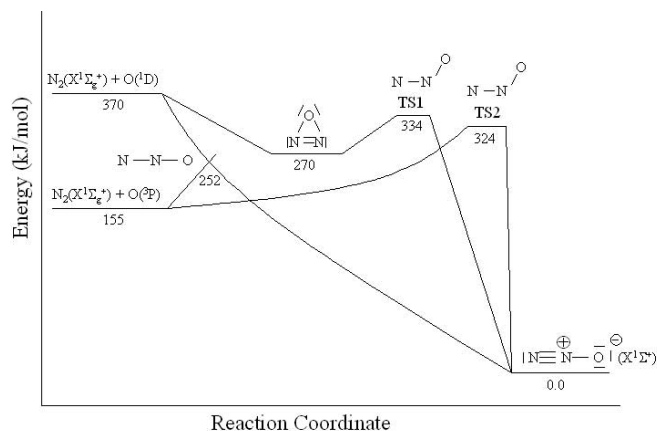


FIG. 12.—PES of the reaction between molecular nitrogen and an oxygen atom in the electronic ground state ( $^3P$ ) or in the first electronically excited state ( $^1D$ ) to the linear nitrous oxide product on the triplet and singlet manifold.

proceed with a suprathermal oxygen atom in its electronic ground state ( $^3P$ ) on the triplet surface. The lowest energy pathway on the triplet surface to form the nitrous oxide molecule passes through a conical intersection that is located 97 kJ mol $^{-1}$  above the reactants; this reaction holds an exoergicity of 155 kJ mol $^{-1}$ . Alternatively, atomic oxygen can add to the lone pair of the nitrogen atom and form nitrous oxide via transition state TS2. In any case, the formation of the reaction products requires the involvement of either suprathermal, ground-state oxygen atoms of a kinetic energy of at least 97 kJ mol $^{-1}$  or electronically excited oxygen atoms. This underlines the importance of nonequilibrium chemistry in low-temperature ices to form nitrous oxide molecules.

To understand the primary mechanism responsible for the formation of nitrous oxide, it could be useful to compare the kinetics associated with the formation of nitrous oxide to that of carbon trioxide. As mentioned earlier,  $3.2 \times 10^{14}$  molecules cm $^{-2}$  of nitrous oxide were produced. Comparing this with the  $2.8 \times 10^{16}$  oxygen atoms cm $^{-2}$  that were generated, only about 1% of the oxygen atoms reacted with molecular nitrogen to form linear nitrous oxide, as shown in equation (18). Recalling that about 3% of the oxygen atoms reacted with carbon dioxide to form carbon trioxide, this means that the oxygen atoms are more likely to react with carbon dioxide than they are to react with molecular nitrogen. These data might suggest an enhanced impact parameter of the oxygen atom reacting with the carbon dioxide molecule compared to molecular nitrogen. Here carbon trioxide is formed by an oxygen atom adding to one of the two double bonds on the carbon dioxide molecule, as confirmed by Bennett et al. (2004). This involves trajectories with large impact parameters in which the oxygen atom interacts with the  $\pi$  electron density of the carbon dioxide molecule; trajectories with small or zero impact parameters do not form the carbon trioxide molecule. However, the cone of acceptance and hence the range of reactive impact parameters for a singlet/triplet oxygen atom reacting with a nonbonding electron pair of a nitrogen molecule to form nitrous oxide is smaller than addition of an oxygen atom across one of the two double bonds of carbon dioxide. This could account for the enhanced formation of the carbon trioxide versus nitrous oxide based on an increased range of the reactive impact parameters leading to the final product. This might also suggest the involvement of a significant fraction of suprathermal triplet oxygen atoms, since singlet oxygen can also add to the triple bond of the nitrogen molecule; this would increase the range of acceptable impact parameters

and could yield an enhanced formation of the nitrous oxide compared to the carbon trioxide molecule, which was clearly not observed in our experiments.

We now investigate why the reaction of oxygen with molecular nitrogen occurs faster than reaction with carbon dioxide. If only electronically excited oxygen atoms reacted, then similar reaction rates would be anticipated, simply because the reaction of excited oxygen atoms with nitrogen has no entrance barrier and the competing reaction with carbon dioxide holds only a small barrier of a few kJ mol $^{-1}$ , which can be overcome by electronically excited oxygen atoms and a small fraction of suprathermal oxygen atoms. On the other hand, the reaction of ground-state triplet oxygen with nitrogen involves a barrier of only 97 kJ mol $^{-1}$ , versus a barrier of 148 kJ mol $^{-1}$  in the  $\text{O}(^3P)\text{-CO}_2$  system. A comparison of the experimental formation rate with the electronic structure calculations suggests that because of the lower barrier, a larger fraction of suprathermal oxygen atoms can overcome the entrance barrier involved in the reaction of ground-state oxygen with molecular nitrogen. This also suggests that a significant fraction of the reacting oxygen atoms are in fact in their triplet ground state. We would like to stress that so far we have no means of directly quantifying the contribution of singlet versus triplet oxygen atoms. The primary reaction pathway of ground state versus excited state will be investigated directly in a future work using a tunable ultraviolet synchrotron radiation source to distinguish between a principle reaction with  $\text{O}(^3P)$  and/or  $\text{O}(^1D)$ .

#### 4.3. Energetics

Finally, it is important to examine the energy balance of the experiment. Energy of the incident radiation can be distributed in the ice by breaking bonds, by ionizing molecules, by electronic or vibrational excitations, or by increasing the kinetic energy of the molecules. The contributions to each from the initial radiation energy can be quantified in order to better understand how incident radiation will affect an ice surface. We simulated the interaction of the implanted electrons with the ice target using the Monte Carlo Simulation of Electron Trajectory in Solids (CASINO) program.<sup>6</sup> A homogeneously mixed model ice was used that was equivalent in chemical composition, density, and thickness to the ice in our experiment. This can be justified as follows. Both solid carbon dioxide and nitrogen hold a cubic crystal structure with four molecules per unit cell and lattice constants of 5.54 and 5.66 Å, respectively (Keesom & Kohler 1934; Scott 1976). Since they have a tendency to form similar crystal structures, this indicates that there exist similar electronic charge distributions around each molecule, suggesting that carbon dioxide and nitrogen ices can form homogeneous solutions in the amorphous solid state. Furthermore, we did not observe any lattice bands of crystalline carbon dioxide ice, also supporting a noncrystalline, homogeneous ice sample. The electron bombardment using 5 keV energy electrons was simulated for 100,000 trajectories using four different physical models for the total cross section. The partial cross section was kept constant using “Mott by interpolation,” and the effective section ionization was set to “Casnati.” The model experiment used a homogeneous ice layer that was elementally composed of two nitrogen, one carbon, and two oxygen atoms, where the assumed density was the average density of molecular nitrogen and carbon dioxide (1.36 g cm $^{-3}$ ). A layer thickness of 409 nm was used and irradiated with 5 keV energy electrons with a

<sup>6</sup> See <http://www.gel.usherb.ca/casino/index.html>.

beam radius of 10 nm. These simulations imply that on average,  $2.69 \pm 0.04$  keV of each electron were absorbed in the ice. Accounting for the total number of electrons incident on the ice in the experiment ( $1.8 \times 10^{15}$  electrons), a total energy of  $4.7 \times 10^{18}$  eV was transferred from the electrons to the target. We now compare these data with our experimental observations. Using the number of carbon dioxide and nitrogen molecules destroyed by the irradiation, and accounting for the bond dissociation energy of carbon-oxygen and nitrogen-nitrogen (5.51 and 9.80 eV, respectively), the total energy used for breaking bonds in the experiment is  $(1.6 \pm 0.2) \times 10^{18}$  eV. This value makes up only 33% of the total energy deposited in the ice, indicating that  $3.1 \times 10^{18}$  eV are available for vibrational and electronic excitation, secondary ionization, and the kinetic energy of the released oxygen and nitrogen atoms.

## 5. ASTROPHYSICAL IMPLICATIONS

Understanding the chemistry of nitrogen is important for identifying nitrogen-bearing molecules and following chemical reaction pathways in extraterrestrial environments. One molecule that could be used to trace the infrared-inactive nitrogen molecule is the linear, closed-shell nitrous oxide molecule,  $\text{N}_2\text{O}(X^1\Sigma^+)$ . In this paper we experimentally simulated the formation of nitrous oxide,  $\text{N}_2\text{O}(X^1\Sigma^+)$ , in interstellar space and in ices of Pluto and Triton in a molecular nitrogen ( $\text{N}_2$ )-carbon dioxide ( $\text{CO}_2$ ) ice mixture at 10 K upon Galactic cosmic-ray particle processing. By monitoring the temporal evolution of the  $2235\text{ cm}^{-1}$  absorption band of nitrous oxide, we were able to elucidate the inherent kinetics and reaction dynamics. Our investigations show that upon interaction with  $\delta$ -electrons in the ultra track of Galactic cosmic-ray particles, the carbon dioxide molecule loses an oxygen atom, also forming a carbon monoxide molecule. The kinetics and dynamics indicate that predominantly suprathreshold ground-state oxygen atoms ( $^3P$ ) are formed that have sufficient excess energy to pass the conical intersection, which is located  $97\text{ kJ mol}^{-1}$  above the energy of the separated reactants. This process leads to an addition of the oxygen atom to the nonbonding electron pair of the nitrogen molecule forming the nitrous oxide molecule. In addition, electronically excited oxygen atoms ( $^1D$ ) can interact without barrier with a nonbonding electron pair of the nitrogen molecule on the singlet manifold to also yield the nitrous oxide molecule. Formed on interstellar grains in cold molecular clouds, the nitrous oxide molecule can be released into the gas phase once the hot core stage has been

reached. Therefore, the  $\text{N}_2\text{O}(X^1\Sigma^+)$  species can act as a tracer molecule to derive the abundances of the nitrogen molecule in interstellar ices. Our experiment also suggests that  $\text{N}_2\text{O}(X^1\Sigma^+)$  should be observable in the surfaces of Triton and Pluto. Accounting for the simulated processing of the ice samples by Galactic cosmic-ray particles of  $5.3 \times 10^6$  yr and the actual relative abundances of nitrogen to carbon dioxide of about 100 on Triton, we expect column densities of about  $10^{12}$ – $10^{13}\text{ cm}^{-2}$  for the nitrous oxide molecule. However, this estimate is dependent on factors such as ice depth, grain size, crystal structure, molecular homogeneity of the ice, and depth-dependent energy deposition, as well as many other variables, so this estimated column density is only rough. Nonetheless, this should assist a prospective identification of nitrous oxide on the surfaces of Pluto and Triton.

Aside from being a tracer molecule for the molecular nitrogen abundance, nitrous oxide has also been proposed as a biomarker in planetary atmospheres. The gas is produced by bacterial denitrification in oceans and soils and has little to no abiotic production routes (Churchill & Kasting 2000). However, our study shows that nitrous oxide should be readily produced on interstellar ices, and after cosmic dust infall into a planetary atmosphere, the ice can sublime releasing nitrous oxide into the gas phase. In addition, nitrous oxide can be formed within the planetary atmosphere via irradiation of molecules in the gas phase or on aerosols, as is possible in the atmosphere of Titan. The main atmospheric component of Titan is the nitrogen molecule, but there also exist oxygen-bearing compounds like carbon monoxide and carbon dioxide. Radiation-induced chemistry between molecular nitrogen and a carbon dioxide molecule on aerosol surfaces is likely to produce nitrous oxide on Titan. These are abiotic pathways to arrive at nitrous oxide in planetary atmospheres, and therefore its detection may not be a unique biomarker. Other molecules that demonstrate nonequilibrium chemistry such as ozone, molecular oxygen, or methane should be detected before the observation should be taken as biogenic activity.

This work was supported by PPARC (UK; R. I. K.), the University of Hawaii at Manoa (USA; C. S. J., R. I. K.), Osaka Vacuum (Japan; R. I. K.), and by the NASA-Astrobiology Institute at the University of Hawaii (C. J. B. and R. I. K.). We are also grateful to Ed Kawamura and Dave Kempton (both University of Hawaii, Department of Chemistry) for their electrical and mechanical work.

## REFERENCES

- Anicich, V. G., & Huntress, W. T., Jr. 1986, *ApJS*, 62, 553  
 Baratta, G. A., Domingo, M., Ferini, G., Leto, G., Palumbo, M. E., Satorre, M. A., & Strazzulla, G. 2003, *Nucl. Instrum. Methods Phys. Res. B*, 209, 283  
 Benit, J., Bibring, J. P., & Rocard, F. 1988, *Nucl. Instrum. Methods Phys. Res. B*, 32, 349  
 Bennett, C. J., Jamieson, C. S., Mebel, A. M., & Kaiser, R. I. 2004, *Phys. Chem. Chem. Phys.*, 6, 735  
 Benson, B. D., & Francisco, J. S. 1995, *Chem. Phys. Lett.*, 233, 335  
 Bernstein, M. P., & Sandford, S. A. 1999, *Spectrochim. Acta A*, 55, 2455  
 Chamley, S. B., & Rodgers, S. D. 2002, *ApJ*, 569, L133  
 Churchill, D., & Kasting, J. 2000, in *Darwin and Astronomy: The Infrared Space Interferometer (ESA SP-451; Noordwijk: ESA)*, 183  
 Cruikshank, D. P., Roush, T. L., Owen, T. C., Geballe, T. R., de Bergh, C., Schmitt, B., Brown, R. H., & Bartholomew, M. J. 1993, *Science*, 261, 742  
 Delitsky, M. L., & Lane, A. L. 2002, *J. Geophys. Res.*, 107(E11), 3  
 d'Hendecourt, L. B., Allamandola, L. J., Grim, R. J. A., & Greenberg, J. M. 1986, *A&A*, 158, 119  
 Ehrenfreund, P., d'Hendecourt, L., Dartois, E., Jourdain de Muizon, M., Breitfellner, M., Puget, J. L., & Habing, H. J. 1997, *Icarus*, 130, 1  
 Elsila, J., Allamandola, L. J., & Sandford, S. A. 1997, *ApJ*, 479, 818  
 Gerakines, P. A., Schutte, W. A., & Ehrenfreund, P. 1996, *A&A*, 312, 289  
 Gerakines, P. A., Schutte, W. A., Greenberg, J. M., & van Dishoeck, E. F. 1995, *A&A*, 296, 810  
 Gibb, E. L., Whittet, D. C. B., Boogert, A. L. A., & Tielens, A. G. G. M. 2004, *ApJS*, 151, 35  
 Halfen, D. T., Apponi, A. J., & Ziurys, L. M. 2001, *ApJ*, 561, 244  
 Herbst, E. 2002, *Highlights Astron.*, 12, 55  
 Hudson, R. L., & Moore, M. H. 2002, *ApJ*, 568, 1095  
 Hwang, D., & Mebel, A. M. 2000, *Chem. Phys.*, 259, 89  
 Jacox, M. E., & Milligan, D. E. 1971, *J. Chem. Phys.*, 54, 919  
 Kaiser, R. I. 2002, *Chem. Rev.*, 102, 1309  
 Kaiser, R. I., Gabrysch, A., & Roessler, K. 1995, *Rev. Sci. Instrum.*, 66, 3058  
 Keesom, W. H., & Kohler, J. W. L. 1934, *Physica*, 1, 655  
 Klinger, J., Benest, D., Dollfus, A., & Smoluchowski, R., eds. 1985, *Ices in the Solar System* (Dordrecht: Reidel)  
 Knauth, D. C., Andersson, B.-G., McCandliss, S. R., & Moos, H. W. 2004, *Nature*, 429, 636  
 Krim, L. 1998, *J. Mol. Struct.*, 471, 267  
 Le Teuff, Y. H., Millar, T. J., & Markwick, A. J., 2000, *A&AS*, 146, 157  
 Moll, N. G., Clutter, D. R., & Thompson, W. E. 1966, *J. Chem. Phys.*, 45, 4469

- Moore, M. H., Donn, B., Khanna, R., & A'Hearn, M. F. 1983, *Icarus*, 54, 388
- Nejad, L. A. M., Williams, D. A., & Charnley, S. B. 1990, *MNRAS*, 246, 183
- Owen, T. C., et al. 1993, *Science*, 261, 745
- Pickles, J. B., & Williams, D. A. 1977, *Ap&SS*, 52, 453
- Sandford, S. A., Bernstein, M. P., Allamandola, L. J., Goorvitch, D., & Teixeira, T. C. V. S. 2001, *ApJ*, 548, 836
- Scott, T. A. 1976, *Phys. Rep.*, 27, 89
- Shimanouchi, T. 1977, *J. Phys. Chem. Ref. Data*, 6, 993
- Smith, M. A. H., Rinsland, C. P., Fridovich, B., & Rao, K. N. 1985, *Molecular Spectroscopy: Modern Research*, Vol. 3 (London: Academic)
- Snow, T. P. 2004, *Nature*, 429, 615
- Sodeau, J. R., & Withnall, R. 1985, *J. Phys. Chem.*, 89, 4484
- Steinfeld, J. I., Francisco, J. S., & Hase, W. L. 1989, *Chemical Kinetics and Dynamics* (Englewood Cliffs: Prentice-Hall)
- Stirling, A., Papai, I., Mink, J., & Salahub, D. 1994, *J. Chem. Phys.*, 100, 2910
- Strazzulla, G., Baratta, G. A., & Palumbo, M. E. 2001, *Spectrochim. Acta A*, 57, 825
- Tryka, K. A., Brown, R. H., Anicich, V., Cruikshank, D. P., & Owen, T. C. 1993, *Science*, 261, 751
- Tryka, K. A., Brown, R. H., Cruikshank, D. P., Owen, T. C., Geballe, T. R., & DeBergh, C. 1994, *Icarus*, 112, 513
- Wang, F., Larkins, F. P., Brunger, M. J., Michalewicz, M. T., & Winkler, D. A. 2001, *Spectrochimica Acta A*, 57, 9
- Womack, M., Ziurys, L. M., & Wyckoff, S. 1992, *ApJ*, 393, 188